Design and Control of a Flexible Joint as a Hydraulic Series Elastic Actuator For Manipulation Applications

Xuepeng Cao
School of Construction Machinery, Chang'an University,
Xi'an, China 710064
Automation Technology and Mechanical Engineering Unit, Tampere University,
Tampere, Finland FI-33101
xuepeng.cao@tuni.fi

Mohammad M. Aref, and Jouni Mattila

Automation Technology and Mechanical Engineering Unit, Tampere University,
Tampere, Finland FI-33101
m.aref@ieee.org, and jouni.mattila@tuni.fi

***Abstract*—Lightweight arms with electrical servomotor drives, such as KUKA's LBR IIWA or Franka Panda, have demonstrated outstanding performance and speed in exoskeletons, prosthesis, and legged robot applications. They all share a similarity in actuation, which is based on series elastic actuators (SEAs). In SEAs, the system benefits from known compliance in the actuation that improves the overall performance, especially in contact with an environment that can have an unknown stiffness in assembly tasks. In some of these cases, harmonic drives or harmonic gears on the power transmission lines create the robot's compliance. For hydraulically actuated SEAs, Pratt and Krupp addressed the SEA challenges for lightweight hydraulic manipulators, such as legged robots and wearable power assist equipment. However, this paper focuses on the design and control architecture of SEAs in heavy-duty manipulation with consideration of the load dynamics of hydraulic actuation with variable stiffness or damping of hydraulic fluid with adjustable flexibility. This system faces challenging issues of payload dynamics and compressibility of fluids in a fifth-order dynamic system. In this paper, the hydraulic SEA concept is designed and modeled, and the fifth-order state space SEA model is state feedback controlled in a free space motion to demonstrate the load dynamics of hydraulic actuation. In addition, a P controller and a controller based on integral of time-weighted absolute error (ITAE) are designed. The simulation results show the latter has better performance in the spring deflection of the SEA. A mixed working condition that changes from a purely inertia payload to inertia and an elastic reaction force is designed to examine the switching smoothness for varying payloads, and the control adaptability of the controllers in different working conditions.**

Keywords— Elastic Actuator, Heavy Duty Manipulation

I. INTRODUCTION

With the rapid development and broad applications of robotics, robots are encountering many unstructured environments, in which the robots' interactions with the external environment are unpredictable. Thus, applications of robots such as exoskeletons, prosthesis robots, and legged robots are necessary. How to adapt, and how to work stably and smoothly in these uncertain environments, is highly valued.

Series elastic actuators (SEAs), in which a series spring is placed between the power output shafts of the actuators and the end that interacts with the environment, consist of a drivetrain subassembly and an output carriage subassembly. Compared to traditional actuators (including pneumatic, hydraulic, electric motor, etc.), SEAs have the desired force control, high force fidelity, minimum impedance, and large dynamic range [1, 2]. There are two types of SEAs: electric SEAs and hydraulic SEAs. The former has less power and mass, and more rapid speed, which is suitable for light-duty manipulation, and SEAs have been developed for biomimetic walking robots [3, 4], humanoids [5], and prosthesis robots [6]. The latter type has more power and mass, and slower moving speed, and has significant merits in heavy-duty manipulation; applications include heavy haul transport robots and construction site robots. The hydraulic fluid's compressibility, hydraulic stiffness changes when the piston moves, load variations, and operating point switching induce highly nonlinear dynamic characteristics of hydraulic SEAs. Several control performances of SEAs impacted by internal parameters and payload features have been studied. In [3], a fixed load and a free end with a zero load of a second-order linear actuator model for SEAs was built, and the nonlinear effects of the motor saturation and the operation of the actuator influenced by the spring were analyzed. A force controllable hydro-elastic actuator has been presented. PI feedback was used to control the spring force of the SEAs, which demonstrated the placed spring achieved good force control and low impedance [7]. To understand the environment-adaptive force control characteristics of SEAs, the stability of human-adaptive control was analyzed in very different environments. The convergence precision may degrade as the environment stiffness decreases [8]. Nicholas *et al*. [9] proposed using high motor voltage coupled with an efficient drivetrain to output a large continuous actuator force, while retaining speed, and achieving high performance, especially on high power and force output in a small and lightweight form factor.

In summary, the above-mentioned researchers have done much work on the force controls of SEAs. However, most focused on lightweight power output. In addition, for hydraulically actuated SEAs, the performance of a single element was the main concern, while the impact of the driving power elements, such as a valve-controlled piston, has not been fully considered, such as considerable variation in the hydraulic stiffness or damping with piston movement [10], has strong nonlinear features that greatly affect the performance of SEAs. In Robinson and Pratt's research [3], a lightweight legged robot application, the "Flamingo," was considered. In [3], a hydraulic cylinder was modeled as an integrator without considering the equation of motion or fluid compressibility, which would result in the well-known third-order linear model for the hydraulic servo-valve-driven

This work was partially supported by the Central Universities Funds of Chang'an University under the project "Performances of closed-loop control hydraulic power and application under subsea," Grant No. 300102258201.

actuator [11]. They added a first-order lag to this integrator model to describe the servo-valve dynamics. Thus, the Pratt's model for controller development was second order. However, his assumptions were well justified, because in the paper he emphasized the rapid response of the SEA, and the resulting hydraulic SEA bandwidth was reported to approach a servo valve's bandwidth of 200 Hz (the Moog servo valve). Thus, the Moog servo valve was a limiting factor. For real-world heavy-duty hydraulic manipulator applications, such as excavators or material loaders, the system and actuator hydraulic resonance is between 0.5 and 10 Hz, which is very easy to witness, if a pressure transducer is used to monitor the lowest pressure oscillation frequency. Due to the low-cost requirements, mobile hydraulic valves are widely used in these applications with a valve spool bandwidth of a few Hertz. Therefore, unlike in previous works, such as [3] or [7], in the present case, fluid compressibility must be included in the modeling, which results in a fifth-order linear model, in which the hydraulic servo valve bandwidth is higher than 100 Hz, and thus, can be necklaced.

The SEA system test case is illustrated in Fig.1, which is under investigation for further development. In this paper, we evaluate the closed-loop system in free motion, as well as in encounters with soft contact with external objects.

II. Hydraulic Sea Modeling and Design

To discover the dynamic control characteristics of hydraulic SEAs, the motion characteristics are obtained first. A hydraulic series elastic actuator model based on the prototype described above is established, as shown as Fig.1. The design parameters of the prototype are illustrated in Fig.2.

The servo-valve flows are given as following by the linear flow equation for the spool orifice and the flow continuity equation for the hydraulic cylinder:

$$q_L = K_q x_v - K_c p_L \tag{1}$$

$$q_L = A_p \dot{x}_p + C_{tp} p_L + \frac{V_t}{4\beta_e} \dot{p}_L \tag{2}$$

where q_L and p_L are the load flow and the load pressure difference, respectively. $q_L = (q_1 + q_2)/2$, in m^3/s, and q_1 and q_2 are the forward and return flows, m^3/s, respectively. $p_L = p_1 - p_2$, and p_1 and p_2 are the forward and return pressures, in pascal units, respectively. x_v is the valve displacement from neutral, in meters. K_q and K_c are the valve flow gain and the valve flow coefficient. x_v, x_p, and x_L are the spool displacement, piston displacement, and load displacement, in meters, respectively. $C_{tp} = C_{ip} + C_{ep}/2$ is the total leakage coefficient of the piston, C_{ip} and C_{ep} are the internal leakage coefficient of the piston and the external leakage coefficient of the piston, in cubic meters per pressure.

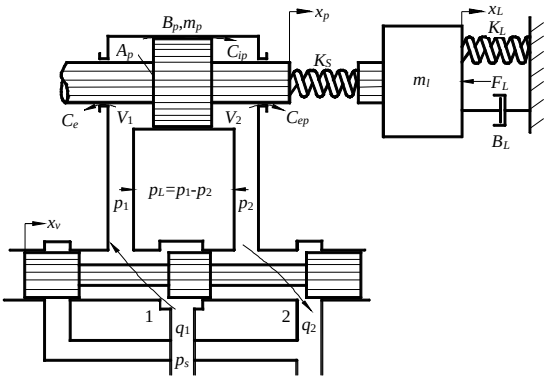

Fig. 2. Schematic diagram of the series elastic actuator.

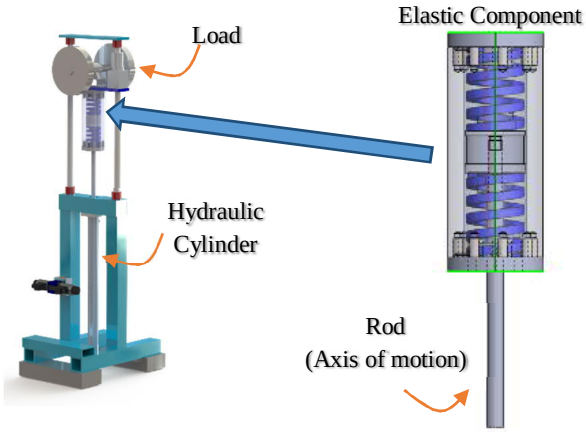

Fig. 1. Prototype of a hydraulic series elastic actuator (SEA). A 20 MPa pressure source is connected to a servo valve. The actuator rod acts on a series spring (zoomed at right), which outputs the spring force to drive the load motivation. The spring compression is measured with a linear potentiometer that implies force.

V_t is the total volume of the fluid under compression in both chambers, in cubic meters. β_e is the effective bulk modulus of the hydraulic oil, in megapascal units.

Considering the output carriage and the drivetrain consist of the two-degrees-of-freedom system in Fig.2, the dynamical equation is written as

$$m_L \ddot{x}_L + B_L \dot{x}_L + (K_S + K_L) x_L - K_S x_p + F_L = 0 \tag{3}$$

$$m_p \ddot{x}_p + B_p \dot{x}_p + K_S x_p - K_S x_L - A_p p_L = 0 \tag{4}$$

where m_p, m_l and m_L are the piston mass, load mass, and load mass, in kilograms, respectively. B_p and B_L are the viscous damping coefficient of the piston and the load, in newton meters per second, respectively. K_L and K_S are the spring stiffness of the load and the actuator, in newton meters, and F_L is the arbitrary load force applied on the actuator, in newtons.

Combining equations (1) and (2), we can obtain the following equation:

$$\frac{V_t}{4\beta_e} \dot{p}_L + K_{ce} p_L + A_p \dot{x}_p - K_q x_v = 0 \tag{5}$$

where $K_{ce} = C_{tp} + K_c$.

Choosing the state vectors as

$$x^T = [x_1 \quad x_2 \quad x_3 \quad x_4 \quad x_5] = [x_L \quad x_p \quad \dot{x}_L \quad \dot{x}_p \quad p_L] \tag{6}$$

equations (3) through (5) in the state space can be denoted as

$$\begin{aligned}
\dot{x}_1 &= x_3 \\
\dot{x}_2 &= x_4 \\
\dot{x}_3 &= -\frac{K_L + K_S}{m_L} x_1 + \frac{K_S}{m_L} x_2 - \frac{B_L}{m_L} x_3 - \frac{1}{m_L} v \\
\dot{x}_4 &= \frac{K_S}{m_p} x_1 - \frac{K_S}{m_p} x_2 - \frac{B_p}{m_p} x_4 + \frac{A_p}{m_p} x_5 \\
\dot{x}_5 &= -\frac{4\beta_e A_p}{V_t} x_4 - \frac{4\beta_e K_{ce}}{V_t} x_5 + \frac{4\beta_e K_q}{V_t} u
\end{aligned} \tag{7}$$

where the controllable input is $u = x_v$, and the interferential input is $v = F_L$.

The equations set (7) can be written in matrix form:

$$\dot{x} = Ax + Bu + Rv \tag{8}$$

$$y = Cx + Du \tag{9}$$

in which, $C = [1 \quad 0 \quad 0 \quad 0 \quad 0]$, $D = [0]$ and

$$A = \begin{bmatrix} 0 & 0 & 1 & 0 & 0 \\ 0 & 0 & 0 & 1 & 0 \\ -\frac{K_L + K_S}{m_L} & \frac{K_S}{m_L} & -\frac{B_L}{m_L} & 0 & 0 \\ \frac{K_S}{m_p} & -\frac{K_S}{m_p} & 0 & -\frac{B_p}{m_p} & \frac{A_p}{m_p} \\ 0 & 0 & 0 & -\frac{4\beta_e A_p}{V_t} & -\frac{4\beta_e K_{ce}}{V_t} \end{bmatrix},$$

$$B = \left[0, 0, 0, 0, \frac{4\beta_e K_q}{V_t}\right]^T, R = \left[0, 0, -\frac{1}{m_L}, 0, 0\right]^T.$$

Considering the actual working conditions, the model above can be divided into the different effects of the payloads.

A. Purely Inertia Payload

In actual application, K_L is often absent, and B_L is very small. Thus, matrix A above becomes

$$\tilde{A} = \begin{bmatrix} 0 & 0 & 1 & 0 & 0 \\ 0 & 0 & 0 & 1 & 0 \\ -\frac{K_S}{m_l} & \frac{K_S}{m_l} & 0 & 0 & 0 \\ \frac{K_S}{m_p} & -\frac{K_S}{m_p} & 0 & -\frac{B_p}{m_p} & \frac{A_p}{m_p} \\ 0 & 0 & 0 & -\frac{4\beta_e A_p}{V_t} & -\frac{4\beta_e K_{ce}}{V_t} \end{bmatrix}.$$

Choosing the load displacement x_L as the output y(t), and neglecting the external load force F_L, we then can obtain the state-space form for hydraulic SEAs:

$$\dot{x} = \tilde{A}x + Bu. \quad (10)$$

B. Inertia and Elastic Payloads

In this case, the payloads including inertia and the external load force (the environment contact) are large enough. Meanwhile, the elastic spring force exerts on the mass m_L; that is, the input F_L, appears. Therefore, equations (8) and (9) and the coefficient matrixes are revised as

$$\dot{x} = Ax + \hat{B}\hat{u} \quad (11)$$

$$y = Cx + \hat{D}\hat{u} \quad (12)$$

where

$$\hat{u} = \begin{bmatrix} u \\ v \end{bmatrix} = \begin{bmatrix} x_v \\ F_L \end{bmatrix}$$

$$\hat{B} = \begin{bmatrix} 0 & 0 \\ 0 & 0 \\ 0 & -\frac{1}{m_L} \\ 0 & 0 \\ \frac{4\beta_e K_q}{V_t} & 0 \end{bmatrix}, \hat{D} = [0 \quad 0].$$

III. CONTROL DESIGN FOR HYDRAULIC SEAS

A. Equivalent Spring Stiffness and Natural Frequency

To investigate the merits of placing a spring between the pistons and to understand how to choose its stiffness, the equivalent spring stiffness consists of the hydraulic spring of the piston and a traditional spring in series, shown in Fig.3.

1) Equivalent Spring Stiffness

In Fig.3, hydraulic spring K_h is in series with the spring K_S, and the equivalent spring stiffness K_e can be denoted as

$$\frac{1}{K_e} = \frac{1}{K_h} + \frac{1}{K_S}. \quad (13)$$

From (13), the equivalent stiffness is limited to the range of $[\frac{K_h K_S}{K_h + K_2}, K_S]$ by placement in the series spring, which limits the variation in the stiffness to a narrow range and improves the system response to external load dynamics.

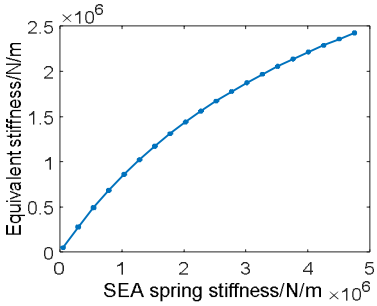

Fig. 3. K_e Versus K_S when $K_h = K_{hmin} = 4.95 \times 10^6$ N/m.

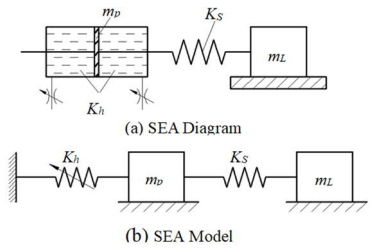

Fig. 4. Simplified model of the hydraulic SEA.

The hydraulic stiffness K_h is given as [10,11]. If the pipes' volumes of the cylinder inlet and outlet are much smaller, compared with the chamber volume of the piston, then the lowest natural frequency occurs when the piston is centered. Correspondingly, the lowest hydraulic stiffness appears at this location, denoted as

$$K_{h\min} = \frac{4\beta_e A_p^2}{V_t}. \quad (14)$$

For choosing the SEA equivalent spring stiffness, a large force bandwidth requires a high spring constant, while minimizing the nonlinear friction and impedance requires a low spring constant [3]. In this paper, we focus on the heavy-duty manipulation application. The parameter values in the calculation are shown in Table 1. Substituting the parameters into equation (14), we can obtain the lowest hydraulic stiffness, $K_{hmin} = 4.95 \times 10^6$ N/m. In addition, the equivalent spring stiffness K_e versus the SEA spring stiffness K_S when $K_h = K_{hmin}$ is plotted in Fig.4.

From Fig.4, we can find that the equivalent spring stiffness K_e is lower than the lowest natural frequency K_{hmin} due to the placement of the spring in the actuator. For example, when $K_S = K_{hmin} = 4.95 \times 10^6$ N/m, $K_e = 2.5 \times 10^6$ N/m is only half of the K_{hmin}. Considering that the purpose of the SEA design is to decrease the actuator stiffness for improvement in the contact force controllability, the mechanical spring stiffness K_S is chosen to be smaller than the hydraulic spring stiffness. Thus, K_{hmin} can be seen as the upper bound of the elastic spring stiffness. In addition, the decrease in the spring stiffness represents the decrease in the equivalent natural frequency, while narrowing the bandwidth deteriorates the rapid response in the SEA's motion or force. For example, if $K_S = 0.01\ K_{hmin}$ and $K_{hmin} = 4.95 \times 10^4$ N/m, then $K_e = 4.90 \times 10^4$ N/m. According to (15) and Fig.5, the equivalent natural frequency w_e will decrease about 1/10 times compared with that of the traditional actuator and approaches the minimum acceptable break point. Therefore, the lower bound is set to be $0.01\ K_{hmin}$. Thus, the reasonable limits for the spring stiffness K_s of the series elastic spring is chosen as $[0.01\ K_{hmin}, K_{hmin}]$.

2) Natural Frequency

The equivalent natural frequency of the SEA can be depicted as

$$\omega_n = \sqrt{\frac{K_e}{m_e}} = \frac{1}{\sqrt{\frac{M_t}{K_h} + \frac{m_L}{K_S}}} = \frac{1}{\sqrt{\frac{1}{\omega_h^2} + \frac{1}{\omega_L^2}}} \quad (15)$$

$$\omega_h = \sqrt{\frac{K_h}{M_t}}, \omega_L = \sqrt{\frac{K_S}{m_L}} \quad (16)$$

where m_e represents the equivalent mass consisting of the total mass M_t, including the piston and the load.

Similarly, the equivalent natural frequency varies with the spring stiffness, changing from 4.95×10^4 N/m to 4.95×10^6 N/m, that is, from $0.01K_{hmin}$ to K_{hmin}, as shown in Fig.5. Connecting two elastic components in series reduces the effective stiffness, and therefore, lowers the natural frequency from 2.5 Hz to 17.5 Hz, with the decrease in the spring

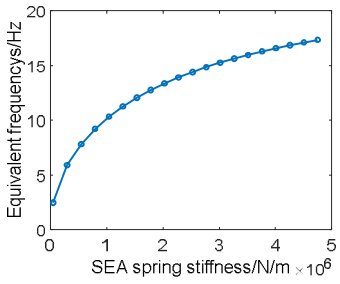

Fig. 5. ω_e versus K_S when $K_h = K_{hmin} = 4.95 \times 10^6$ N/m.

stiffness. This can mean the bandwidth is partially compromised for smoothness in the system response. For heavy-duty manipulators with a low natural frequency, the system or actuator hydraulic resonance of excavators or material loaders is between 0.5 and 10 Hz. This compromise in the bandwidth of the actuators does not cause a problem, because the actuator is fast enough for the application. However, 2.5 Hz approaches the minimum acceptable break point, seen as the lower bound of hydraulic SEAs.

B. Controller Design Based on the ITAE Criterion

For this fifth-state space model, the relevant optimal coefficients of the closed-loop transfer function based on the ITAE criterion for step input are shown as follows [12]:

$$R(s) = s^5 + 2.8\omega_n s^4 + 5.0\omega_n^2 s^3 + 5.5\omega_n^3 s^2 + 3.4\omega_n^4 s + \omega_n^5 \quad (17)$$

Suppose $R(s) = 0$; the desired poles can be calculated. By solving pole-placement problems, the corresponding state feedback-gain vector $K = [K_1 \quad K_2 \quad K_3 \quad K_4 \quad K_5]$ can obtained. The designated controller structure is as follows:

$$u = K_1(x_{p_{ref}} - x_{p_{feedback}}) - K_2\dot{x}_{p_{feedback}} + K_3(x_{L_{ref}} - x_{L_{feedback}}) - K_4\dot{x}_{L_{feedback}} - K_5 P_L \quad (18)$$

where the constant parameters should meet $K_1 > K_2 > K_3 > K_4 > K_5$, and whose absolute value is used. In simulations, K_s is set as the lower bound value of the fixed range above $[0.1K_{hmin}, K_{hmin}]$. $K_S = K_{hmin}/10 = 4.95 \times 10^5$ N/m. Then we can compute with equation (16) $\omega_h = \omega_{hmin} = 155.36$ rad/s (24.7 Hz) and ω_L=49.63 rad/s (7.9 Hz), and the natural frequency can be calculated $\omega_n = 47.39$ (7.5Hz) through equation (15).

Substituting into (17), the numeric ITAE polynomials are obtained as $R(s) = s^5 + 132.3627s^4 + 1.1173 \times 10^4 s^3 + 5.8101 \times 10^5 s^2 + 1.6979 \times 10^7 s + 2.3607 \times 10^8$.

Let $R(s) = 0$; the desired five poles of the closed-loop transfer function are computed as

$$s = -17.7938 \pm 61.0740i, -42.3326, -27.2213 + 25.24i.$$

To place the poles at the above desired places, the feedback-gain vector is determined as follows:

$K = [2.4\times10^{-3}\ -2.4\times10^{-3}\ 2.26\times10^{-5}\ -2.51\times10^{-4}\ 1.62\times10^{-12}]$. The designated corresponding controller structure is as follows:

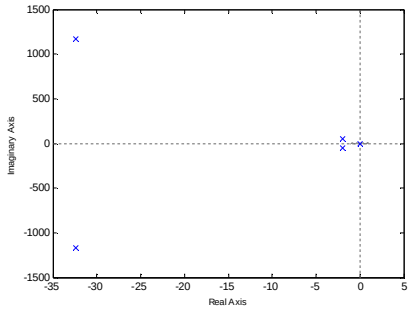

Fig. 7. The poles distribution for SEA system when $K_S = 4.95 \times 10^5$ N/m.

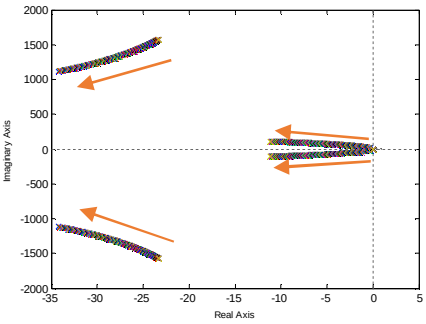

Fig. 6. The pole distribution for the hydraulic SEA system when K_S varies from 4.95×10^4 N/m to 4.95×10^6 N/m.

$$u = 2.4 \times 10^{-3} \times (x_{p_{ref}} - x_{p_{feedback}}) - 2.4 \times 10^{-3} \times \dot{x}_{p_{feedback}} + 2.51 \times 10^{-4} \times (x_{L_{ref}} - x_{L_{feedback}}) - 2.26 \times 10^{-5} \times \dot{x}_{L_{feedback}} - 1.62 \times 10^{-12} \times P_L \ . \quad (19)$$

IV. SIMULATION AND PERFORMANCE ANALYSIS

The parameter values for the hydraulic SEA system are listed in Table 1. Substituting the parameter numerical values into the coefficient matrixes $\tilde{A}$ and B for purely inertia payloads, then

$$\tilde{A} = \begin{bmatrix} 0 & 0 & 1 & 0 & 0 \\ 0 & 0 & 0 & 1 & 0 \\ -2.4627 \times 10^3 & 2.4627 \times 10^3 & 0 & 0 & 0 \\ 1.2375 \times 10^5 & -1.2375 \times 10^5 & 0 & -25 & 1.3744 \times 10^{-4} \\ 0 & 0 & 0 & -9.0 \times 10^9 & -43.774 \end{bmatrix}$$

$$B = [0 \quad 0 \quad 0 \quad 0 \quad 3.9289 \times 10^{13}].$$

A. Poles Maps and Root-locus Plots

The pole-zero map is shown in Fig.6, according to matrixes $\tilde{A}$ and B above. Except for one pole at origin (0, 0), all conjugate poles are located in the left side of the S plane. In addition, a pair of conjugate poles is next to the imaginary axis. Thus, this system can be judged to be in the critical steady state. The poles change with spring stiffness K_S, varying from 4.95×10^4 N/m to 4.95×10^6 N/m, shown in

TABLE I. PARAMETER VALUES FOR THE HYDRAULIC SEA ANALYSIS.

Symbols	Value	Components	Symbols	Value	Components
d_1	32×10^{-3}m^2	Hydraulic cylinder	K_q	2.4 m^2/s	Servo Valve
d_2	18×10^{-3}m^3		K_c	$2.5 \times 1\ 0^{-12}$ m^3/(Pa . s)	
L	0.4 m		K_S	4.95×10^5 N/m	SEA Spring
m_p	4 kg		K_{hmin}	4.95×10^6 N/m	
B_{pp}	100 N/m/s		m_t	200 kg	Load
C_{ep}	1.16×10^{-13} m^3/(Pa . s)		F_L	3000 N	
C_{ip}	1.16×10^{-13} m^3/(Pa . s)		β_e	9.0×10^8	Hydraulic oil
			ρ	0.88×10^3 kg/m^3	

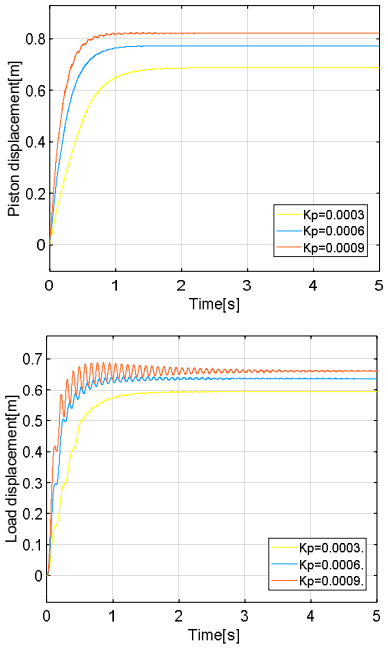

Fig. 8. Step responses of x_p (top) and x_L (bottom) when changing K_p = 3.0×10^{-4}, 6.0×10^{-4} to 9.0×10^{-4} and keeping $K_L = 4.95 \times 10^5$ N/m and $K_S = 4.95 \times 10^5$ N/m

Fig.7. Along with the value K_S increasing, two pairs of conjugate poles move away from the imaginary axis except for the origin pole. This variation reveals the hydraulic SEA with a larger stiffness spring can strengthen the output stability.

B. Step Responses

1) Solution Work Flow

a) P control

When the proportional regulator K_p is used for a closed-loop system, the step response under the unity passive feedback scheme of the state space model for purely inertia payloads is as shown in Fig.8.

b) The controller based on ITAE

The controller used for the closed-loop system denoted by equation (19) in the step response scheme of the state space model for the purely inertia load is shown in Fig.9.

c) Different payload switching conditions

Assuming the hydraulic SEA drives a purely inertial m_L at the initial stage, displacement $l/2$, on which a spring load K_L is exerted, is seen in Fig.10. In Fig.10, two working conditions changing from a purely inertia payload to inertia and elastic payloads are considered. To simulate this situation, the payload is the purely inertia load. At the switching point x_L = 0.5, the load spring force is exerted, whose step response under P control is shown in Fig.11.

C. Analysis of the Simulation Results

1) Purely inertia payload condition

The step responses of x_p and x_L are simulated with the P control and the controller based on ITAE when K_S changes from 4.95×10^4 N/m to 4.95×10^6 N/m, shown in Fig.12 and Fig.13. As shown in Fig.13, when K_p remains constant, less stiffness K_S will more easily result in oscillations of x_L. No matter how the P value is tuned, oscillations of x_L remain when $K_s = 4.95 \times 10^4$ N/m. Therefore, P control is not applicable for small spring stiffness. Once the oscillation disappears,

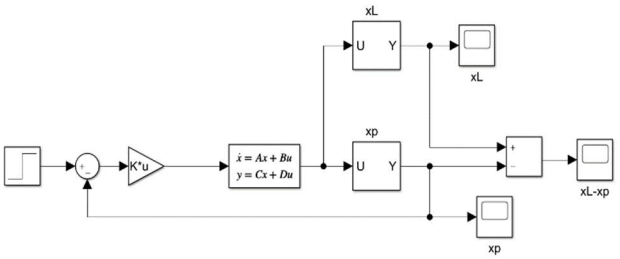

Fig. 10. Step response of the closed-loop control scheme for using the P control Kp. The signal xL is outputted by setting as C = [1 0 0 0 0] through Selector 1, and xp is feedbacked as C = [0 1 0 0 0] in Selector 2.

continually increasing the stiffness no longer affects the dynamic response. When K_S remains constant, degrading K_p from 1/2000 to 1/6000 can gradually restrain the step-response oscillation, and improve the stability performances. However, when K_p decreases further, the responses change from the under-damped state to the over-damped state. Compared with the considerable influence on x_L, the changing stiffness K_S has minor impacts on the step-response x_p, shown in Fig.12.

The control performances under the ITAE controller compared using P control, no matter the step responses of x_p or x_L, approach the optimal performances, regardless of the changes in K_S, which shows it has good robustness to overcome the variation in the stiffness of the SEA spring. This result shows that the controller based on ITAE criteria is conducted to validate the control convergence and indices suited to different spring stiffnesses.

2) Different payload switching conditions

According to the payload switching and resolution block shown in Fig.10 and Fig.11, step response results can be obtained when any coefficient changes in the parameters set [K_L, K_S, K_p].

Next, as Fig.14 shows, across the switching point x_L = 0.5, the increasing rate of x_p or x_L slows until it approaches the stable state, when $K_L \neq 0$. With K_L increasing, the steady value of x_p decreases, and the steady-state error has few changes. When K_L is very big, such as $K_L = 4.95 \times 10^{20}$ N/m, the steady value approaches x_p = 0.679. At the switching point, the displacement x_p will appear as a short-term fluctuation, and then tend to be stable when K_L is less than 4.95×10^5 N/m, and show that continuous high-frequency and low-amplitude vibration occur when K_L is greater than it. This is because the working condition changes from the purely inertia payload to the inertia and elastic payloads.

As Fig.15 shows, after the switching point x_L= 0.5 is crossed, the increasing tendencies of x_p or x_L with K_S increasing are similar to the varying K_L mentioned above. However, the small spring stiffness of the SEA, such as K_S = 4.95×10^4 N/m, easily induces a big oscillation in the load displacement x_L. With the increasing K_S, the stable value of x_L becomes larger; meanwhile, the oscillation vanishes gradually. Fig.16 demonstrates, with increasing K_p, the stable performance of x_p or x_L gets better, oscillation is depressed, and the stable values become small.

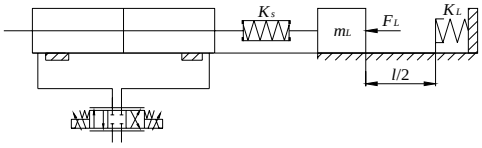

Fig. 9. Classical working conditions for the application of the hydraulic SEA.

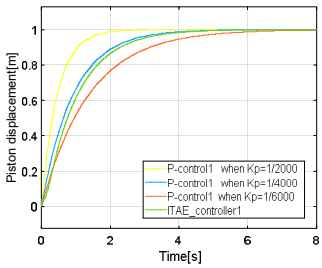

(1) $K_S = 4.95 \times 10^4$ N/m

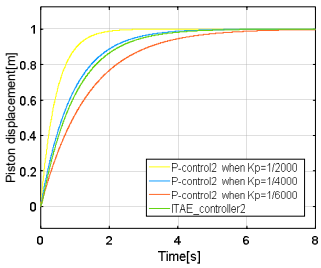

(2) $K_S = 4.95 \times 10^5$ N/m

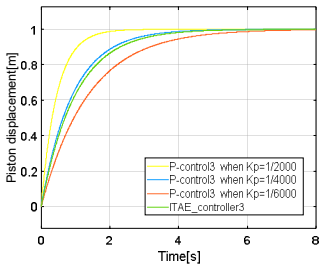

(3) $K_S = 4.95 \times 10^6$ N/m

Fig. 11. Step responses of piston displacement x_p compared using the P control K_p with the controller based on ITAE.

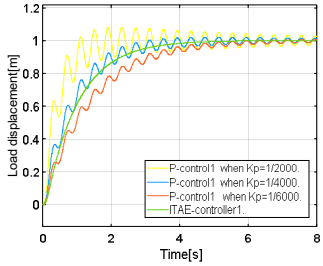

(1) $K_S = 4.95 \times 10^4$ N/m

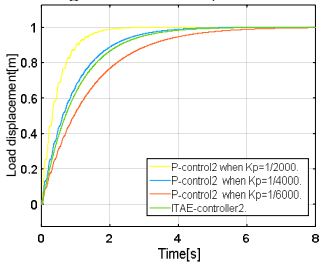

(2) $K_S = 4.95 \times 10^5$ N/m

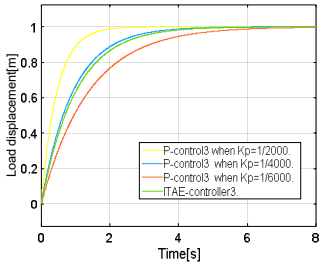

(3) $K_S = 4.95 \times 10^6$ N/m

Fig. 12. Step responses of load displacement x_L compared using the controller K_p with the controller based on ITAE.

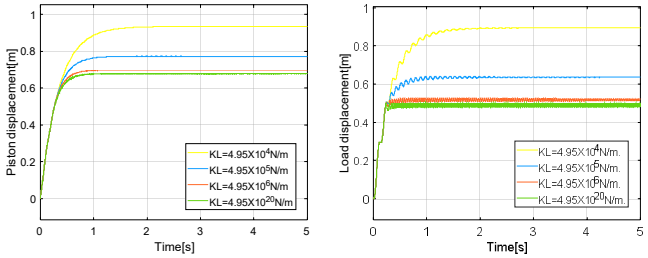

Fig. 13. Step responses of x_p and x_L when changing $K_L = 4.95 \times 10^4$ N/m, 4.95×10^5 N/m, 4.95×10^6 N/m to $K_L = 4.95 \times 10^{20}$ N/m and keeping $K_S = 4.95 \times 10^5$ N/m and $K_p = 6.0 \times 10^{-4}$. The external compliance force is exerted at the moment the displacement reaches 0.5 m.

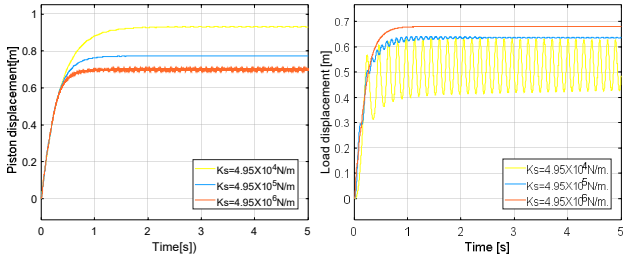

Fig. 14. Step responses of x_p and x_L when changing $K_S = 4.95 \times 10^4$ N/m, 4.95×10^5 N/m to 4.95×10^6 N/m and keeping $K_L = 4.95 \times 10^5$ N/m and $K_p = 6.0 \times 10^{-4}$.

V. Conclusions

This paper proposes use of flexible coupling in the serial structure of a hydraulic actuator in heavy-duty robotic architectures. Considering the load dynamics of hydraulic power elements, a fifth-order state space SEA that is state feedback controlled in a free space motion is designed and modeled. In addition, P control and the controller based on ITAE are designed for two kinds of payloads, including a purely inertia payload and a mixed payload. The simulation results show the ITAE controller has better control performance for hydraulic elastic spring actuators. In addition, the equivalent spring stiffness and the natural frequency for the hydraulic SEA are computed, and how to choose the spring stiffness for heavy-duty application is proposed. This paper provided insight into the effect of mechanical stiffness in contact, and the spring stiffness K_S is considered to be an adjustable design parameter, depending on the robot's structure or the load dynamics. In addition, a combination of conditions changing from a purely inertia payload to a mixed payload is simulated, which demonstrates the outputs of the displacements of the piston and the load run smoothly at the switching point $x_L = 0.5$ and have suitable control adaptability for changing payloads.

This paper shows that this change in the mechanical structure can act as a design parameter for tuning the overall mechatronic behavior of the system. This modification can play a key role in reconfigurable structures and multipurpose robotic arms. Depending on the design for mechanical flexibility, together with the loop gain of the controller, the load can face stiff or compliant behavior from the robot's actuator. Therefore, the overall system becomes less sensitive to errors, delays, and backlash in instrumentation, control, and actuation. Further developments are under investigation, to provide insight for the design and implementation of variable stiffness actuation for heavy-duty robotic structures with compliance.

References

[1] Pratt, J.E. and Krupp, B.T., 2004, "Series Elastic Actuators for Legged Robots." *Unmanned Ground Vehicle Technology*, International Society for Optics and Photonics, Vol. VI, p. 135.

[2] Pratt, Jerry, Krupp, Ben, and Morse, Chris, 2002, "Series Elastic Actuators for High Fidelity Force Control." *Industrial Robot*, Vol. 29, pp. 234-241.

[3] Robinson, D. W., Pratt, J. E., Paluska, D. J. and Pratt, G. A., 1999, "Series Elastic Actuator Development for a Biomimetic Walking Robot," *IEEE/ASME Conf. on Advanced Intelligent Mechatronics*, pp. 561-568.

[4] Remy, C. D., Siegwart, R., Gehring, C., Bloesch, M., Hoepflinger, M. A., and Hutter, M., 2012, "StarlETH: A Compliant Quadrupedal Robot for Fast, Efficient, and Versatile Locomotion," in *Proceedings of the 15th International Conference on Climbing Walking Robot (CLAWAR 2012)*, Autonomous Systems Lab, ETH Zurich, pp. 1-8.

[5] Lee, B., Knabe, C., Orekhov, V., and Hong, D., 2014, "Design of a Human-Like Range of Motion Hip Joint for Humanoid Robots," in *Proceedings of the ASME International Design Engineering Technical Conference, ASME*, pp.1-8.

[6] Grimmer, M., Eslamy, M., and Seyfarth, A., 2014, "Energetic and Peak Power Advantages of Series Elastic Actuators in an Actuated Prosthetic Leg for Walking and Running." *Actuators*, Multidisciplinary Digital Publishing Institute, Vol. 3, No. 1, pp. 1-19.

[7] Robinson, D. W. and Pratt, G. A., 2000, "Force Controllable Hydro-Elastic Actuator," in *Proceedings 2000 ICRA. Millennium Conference. IEEE International Conference on Robotics and Automation. Symposia Proceedings*, IEEE, Vol. 2, pp. 1321-1327.

[8] Calanca, A. and Fiorini, P., 2018, "Understanding Environment-Adaptive Force Control of Series Elastic Actuators." *IEEE/ASME Transactions on Mechatronics*, Vol. 23, No. 1, pp. 413-423.

[9] Paine, N., Oh, S., and Sentis, L., 2014, "Design and Control Considerations for High-Performance Series Elastic Actuators." *IEEE/ASME Trans. on Mechatronics*, Vol. 19, No. 3, pp. 1080-1091.

[10] Viersma, Taco J., 1980, *Analysis, Synthesis, and Design of Hydraulic Servosystems and Pipelines*.

[11] Merritt, H.E., 1967, *Hydraulic Control Systems*.

[12] Dorf, Richard C., 1992, *Modern Control Systems*.